

CONSTRUCTION OF BALLISTIC LUNAR TRANSFERS LEVERAGING DYNAMICAL SYSTEMS TECHNIQUES

Stephen T. Scheuerle*, Brian P. McCarthy†, and Kathleen C. Howell‡

Ballistic lunar transfers exploit the gravitational influence of the Earth, Moon, and Sun to reduce propellant costs associated with transfers from the Earth to the lunar vicinity via heliocentric space. This investigation considers the computation of lunar transfers in the Circular Restricted Three-body Problem (CR3BP) and the Bicircular Restricted Four-body Problem (BCR4BP). Families of transfers are constructed by leveraging dynamical systems theory techniques. Feasible solutions are delivered that reach various destinations nearby the Moon, including conic and libration point orbits. Additionally, energy properties formulated relative to these models characterize different transfer geometries. These strategies provide insight into the process for selection and construction of ballistic lunar transfers for trajectory design.

INTRODUCTION

In the coming decades, NASA aims to develop a long-term sustainable human presence in cislunar space.^{1,2} One challenge associated with this advancement is the development of propellant efficient paths to access the lunar region. To meet this challenge, this investigation explores ballistic lunar transfers. Ballistic lunar transfers exploit solar gravity to reduce lunar orbit insertion (LOI) costs associated with arrival into the lunar region in exchange for longer times of flight. Thus, they serve as a viable option for transfers when time of flight is flexible. In 1991, JAXA's Hiten spacecraft leveraged such a transfer during a recovery effort for the mission and, in 2011, the Gravity Recovery and Interior Laboratory mission (GRAIL) employed such a transfer to reach low lunar orbit.^{3,4} Similarly, ballistic lunar transfers are being considered for logistics and cargo deliveries to the lunar Gateway.⁵ Ultimately, ballistic lunar transfers offer a viable alternative to direct, higher-cost transfers to the lunar region when time of flight constraints are relaxed.

Various approaches have been employed to compute ballistic lunar transfers. Parker et al. exploit numerical techniques and dynamical systems theory (DST) to characterize ballistic lunar transfers.^{6,7} Parrish et al. investigate the use of ballistic lunar transfers to reach Near Rectilinear Halo Orbits (NRHOs), using numerical methods and DST techniques.⁸ Similarly, Oshima et al. exploit a grid search, coupled with a direct transcription method, to produce ballistic lunar transfer solutions in the Bicircular Restricted Four-body Problem.⁹ This investigation first examines the characteristics of the dynamical environment. The investigation then focuses on employing DST

*Graduate Student, School of Aeronautics and Astronautics, Purdue University, West Lafayette, IN 47907;
sscheuer@purdue.edu

†Ph.D. Student, School of Aeronautics and Astronautics, Purdue University, West Lafayette, IN 47907;
mccart71@purdue.edu

‡Hsu Lo Distinguished Professor, School of Aeronautics and Astronautics, Purdue University, West Lafayette, IN 47907;
howell@purdue.edu. Fellow AAS; Fellow AIAA

techniques to generate individual ballistic lunar transfer solutions. This investigation then illustrates the use of initial guesses to generate and characterize families of ballistic lunar transfers in both the Circular Restricted Three Body Problem and the Bicircular Restricted Four Body Problem. Examining the construction of these transfers within the context of these dynamical models supplies insight into the dynamics driving the availability of these types of transfers under various conditions.

DYNAMICAL MODELS

This investigation employs two models to represent the dynamics in cislunar space. First, motion in the Circular Restricted Three-Body Problem (CR3BP) is examined. Numerous authors have previously applied DST for trajectory design within the context of the CR3BP^{10,11} and this investigation employs some of these techniques in Sun-Earth CR3BP to characterize the lunar ballistic transfer behaviours. However, the end-to-end motion of a ballistic lunar transfer is dependent on three massive bodies. By employing the Bicircular Restricted Four-Body Problem (BCR4BP), techniques from DST are applied to designing trajectories in a model that continuously employs all three massive bodies. The investigation leverages properties and dynamical structures from both the CR3BP and the BCR4BP to construct low energy transfers in cislunar space.

Circular Restricted Three-body Problem

The CR3BP describes the motion of a particle due to the gravitational fields of two massive bodies. The mass of the particle (P_3) is assumed to be negligible compared to the primary bodies (P_1 and P_2), where M_i is the mass of the body P_i . For consistency across systems, P_1 is defined as the more massive body, i.e., $M_1 \geq M_2$. The primaries P_1 and P_2 are modeled as point masses and move in circular orbits about their common barycenter (B_1). By formulating the CR3BP in a coordinate frame that rotates with the primary bodies, the equations of motion are time independent.¹² The rotating coordinate frame is orthonormal, centered about B_1 , and constructed with the $+\hat{x}$ -axis directed towards P_2 , and $+\hat{z}$ -direction is along the orbital angular momentum vector. The vector \vec{r}_{ij} represents the vector from body i to j in the rotating coordinate frame, the position and velocity vectors of P_3 are given by $\vec{r} = (x, y, z)$ and $\dot{\vec{r}} = (\dot{x}, \dot{y}, \dot{z})$ respectively. The vectors are expressed in rotating components. Dots represent derivative with respect to time as a rotating observer. To aid in numerical integration, the problem is nondimensionalized such that both the distance between P_1 and P_2 and the mean motion of the P_1 - P_2 system are set equal to one. Figure 1 provides a visualization of the rotating reference frame with respect to an inertial frame expressed as $(\hat{X}, \hat{Y}, \hat{Z})$. The three scalar nonlinear second-order differential equations that describe the motion of particle P_3 in the rotating frame are,

$$\ddot{x} = 2\dot{y} + \frac{\partial U}{\partial x} \quad (1a) \quad \ddot{y} = -2\dot{x} + \frac{\partial U}{\partial y} \quad (1b) \quad \ddot{z} = \frac{\partial U}{\partial z} \quad (1c)$$

where μ is the mass parameter, defined $\mu = \frac{M_2}{M_1+M_2}$, and defines a CR3BP system. The terms $\frac{\partial U}{\partial x}$, $\frac{\partial U}{\partial y}$, and $\frac{\partial U}{\partial z}$ are the partial derivatives of the pseudo potential function U with respect to the position components of P_3 . The pseudo-potential function, U , is then defined,

$$U = \frac{1}{2} \left(x^2 + y^2 \right) + \frac{1-\mu}{r_{13}} + \frac{\mu}{r_{23}} \quad (2)$$

where r_{ij} is the scalar magnitude of the vector \vec{r}_{ij} . The CR3BP possesses five equilibrium solutions, denoted L_1 through L_5 . The CR3BP also admits a single integral of the motion that represents an ‘energy-like’ quantity, denoted the Jacobi Constant, that remains constant along any ballistic path.¹³

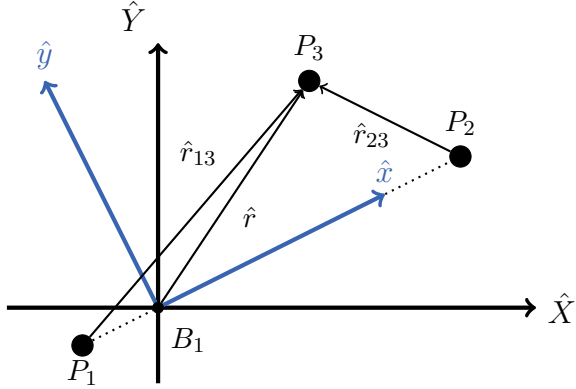


Figure 1. Relationship between the Inertial Reference Frame (black) and the Rotating Reference Frame (blue) for the CR3BP, projected onto the $\hat{x} - \hat{y}$ plane.

As the energy of the spacecraft increases, the value of the Jacobi Constant decreases. The Jacobi Constant is expressed as,

$$C = 2U - (\dot{x}^2 + \dot{y}^2 + \dot{z}^2) \quad (3)$$

The Jacobi Constant also describes the accessible regions for a spacecraft at a given energy level. The boundaries of these accessible regions are denoted the zero velocity surfaces (ZVS) and are defined for a Jacobi Constant value when the relative velocity terms in Equation (3) are set to zero. Thus, for a spacecraft on a ballistic arc in the CR3BP, it remains indefinitely within or beyond a boundary such that the relative velocity components in Equation (3) are real valued. As the Jacobi Constant value increases, the energy decreases and access beyond the P_1 - P_2 neighborhood is increasingly limited. Conversely, as the Jacobi Constant decreases, the energy increases and opens access to transfers through the P_1 - P_2 system. An understanding of the accessible regions provides insight into the energy level that is necessary for ballistic transfer to the Moon.

Bicircular Restricted Four-body Problem¹⁴

The bicircular restricted four-body problem (BCR4BP) describes the motion of a massless particle, P_3 , influenced by the gravitational fields of three massive bodies, i.e., the Earth (P_1), Moon (P_2) and Sun (P_4). The formulation of the BCR4BP is similar to that of the CR3BP, where P_1 and P_2 are assumed to follow circular orbits about their common barycenter B_1 . Additionally, B_1 and P_4 are then modeled in a circular orbit about the total system barycenter B_2 . In this formulation of the BCR4BP model, perturbations induced by P_4 do not influence the motion of P_1 and P_2 . It is advantageous to represent the motion of P_3 in two different rotating coordinate frames, the P_1 - P_2 rotating frame and the P_4 - B_1 rotating frame. The P_1 - P_2 rotating coordinate frame is centered about B_1 , rotates along with P_1 and P_2 , and is constructed with the $+\hat{x}'$ -direction pointing towards P_2 , and the $+\hat{z}'$ -direction is parallel with the orbital angular momentum vector. Figure 2a depicts the P_1 - P_2 rotating reference frame, where the position of P_3 is written as (x', y', z') . The angle θ_s describes the orientation of P_4 with respect to the P_1 - P_2 system, and the dotted circle represents the motion of P_4 . The P_4 - B_1 rotating reference frame locates B_2 as the origin, where the system rotates with the motion of P_4 and B_1 . The frame is orthonormal, and defined with the $+\hat{x}$ -axis directed towards B_1 , and $+\hat{z}$ -axis is along the orbital angular momentum vector of the P_4 - B_1 system. The position of P_3 in the P_4 - B_1 rotating coordinate frame is written as $(\underline{x}, \underline{y}, \underline{z})$. Figure 2b represents the motion

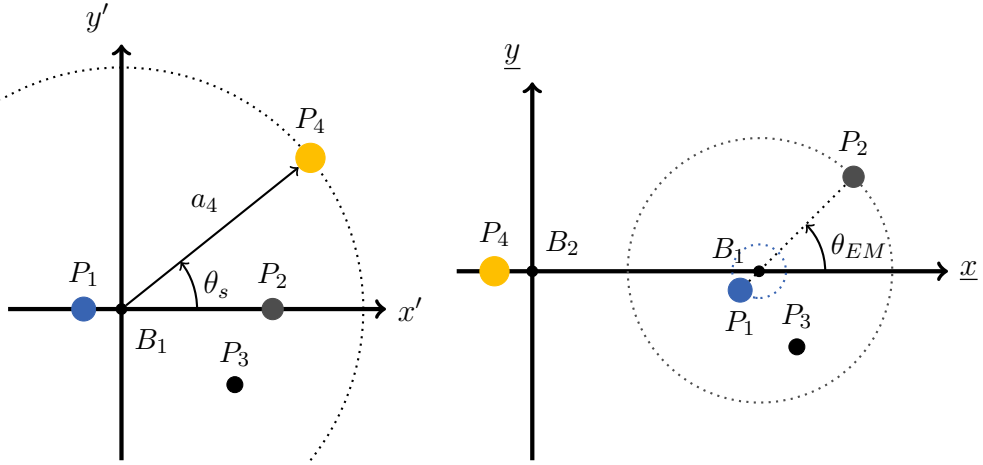


Figure 2. The P_1 - P_2 (a) and P_4 - B_1 (b) rotating coordinate frames in the BCR4BP, not to scale

of the primary bodies in this rotating frame, where the angle θ_{EM} determines the position of P_1 and P_2 , and concentric circles about B_1 describes the motion of P_1 and P_2 . The differential equations are formulated in terms of characteristic quantities to simplify the equations of motion, and reduce errors associated with numerical integration. Similar to the CR3BP, an ‘energy-like’ quantity exists in the BCR4BP,¹⁴ defined as the Hamiltonian, with two useful formulations in either rotating frame. For simplicity, the P_1 - P_2 Hamiltonian is labelled the Hamiltonian and is represented as,

$$H_{P_1 P_2} = 2\Upsilon - V^2 \quad (4)$$

where $V^2 = \dot{x}'^2 + \dot{y}'^2 + \dot{z}'^2$, such that \dot{x}' , \dot{y}' , and \dot{z}' are the relative velocity components of P_3 in the P_1 - P_2 rotating coordinate frame. Then, Υ is the pseudo-potential function in the P_1 - P_2 rotating frame defined as,

$$\Upsilon = \frac{1}{2} \left(x'^2 + y'^2 \right) + \frac{1-\mu}{r_{13}} + \frac{\mu}{r_{23}} + \frac{m_4}{r_{43}} - \frac{m_4}{a_4^3} (x'_4 x' + y'_4 y' + z'_4 z') \quad (5)$$

where μ still represents the mass parameter of the P_1 - P_2 system, m_4 is the nondimensional mass of the Sun such that $m_4 = \frac{M_4}{M_1+M_2}$, a_4 is the semi-major axis of the circular orbit governing the assumed motion of the Sun and B_1 . For the Earth-Moon-Sun system, x'_4 , y'_4 , and z'_4 is the position of the the Sun, defined by an angle θ_s . For the Earth-Moon-Sun system, θ_s orients the Sun as the angle relative to the Sun- B_1 line and increasing for an orientation shifting counter-clockwise in the Earth-Moon rotating frame, associated with the formulation based on the P_1 - P_2 rotating frame. Throughout this investigation, the Earth-Moon Hamiltonian is written as H_{EM} . The governing equations of motion of the Earth-Moon-Sun BCR4BP expressed in the Earth-Moon rotating frame are defined as,

$$\ddot{x} = 2\dot{y}' + \frac{\partial \Upsilon}{\partial x'} \quad (6a) \quad \ddot{y} = -2\dot{x}' + \frac{\partial \Upsilon}{\partial y'} \quad (6b) \quad \ddot{z} = \frac{\partial \Upsilon}{\partial z'} \quad (6c)$$

where Υ is the pseudo potential defined in Equation (5). In this current analysis, the Earth, Moon, and Sun are assumed to be coplanar, i.e., the motion of all three massive bodies is restricted to one plane. From Equation (5), the pseudo-potential function is dependent on a time varying position of the Sun. For a given Sun angle, there exist equilibrium solutions, denoted instantaneous equilibrium solutions. For each orientation of the Sun, there is a different instantaneous equilibrium point and

the equilibrium locations do not remain stationary as the system propagates through time. The instantaneous equilibrium solutions are denoted as E_1 through E_5 . The position of the instantaneous equilibrium solutions in the Earth-Moon rotating frame are displayed in Figure 3a. The curves in Figure 3a represent the collection of discrete instantaneous equilibrium points, where each point is evaluated with zero velocity and acceleration at a unique Sun angle. The Hamiltonian values for all solutions across all Sun angles is displayed in Figure 3b. Note that the locations comprising E_1 always deliver the highest Hamiltonian values, corresponding to the lowest energy, followed by, in terms of increasing energy, E_2 , E_3 , and the E_4 and E_5 pair. For specific Sun angles, E_3 separates into two or three distinct instantaneous equilibrium solutions near 90° and 270° . Also observe that E_2 represents the lowest energy at which a spacecraft can traverse in and out of the Earth-Moon region; thus, the Hamiltonian values for E_2 are relevant when characterizing the motion of ballistic lunar transfers. Using the Hamiltonian written in Equation (4) and setting the relative velocity components to zero, instantaneous ZVS are determined for a given Sun angle. The ZVSs act as a visual representation of the impact of energy in perturbing a spacecraft in the BCR4BP, allowing access to various regions of space due to natural perturbations. Although the BCR4BP is time-variant, the model assumes periodic behaviors of the massive bodies and thus, is not coherent. However, the model incorporates all three bodies governing the transfer geometry for a ballistic lunar transfer into a single, convenient model.

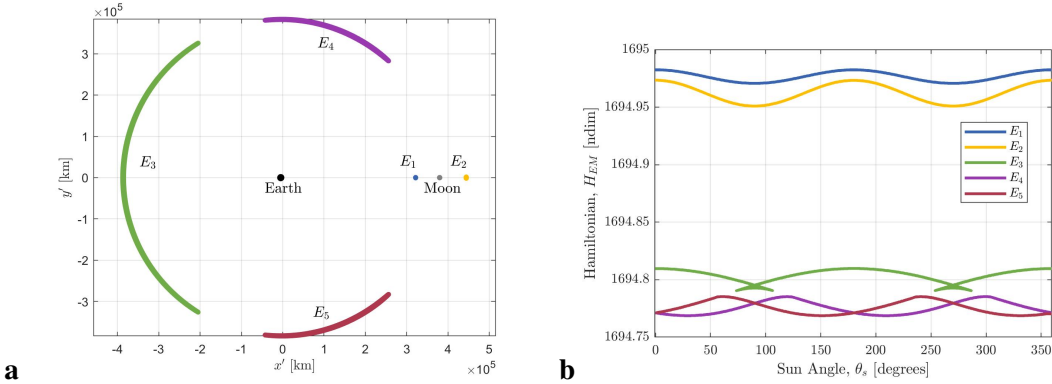


Figure 3. Hamiltonian vs Sun angle for the instantaneous equilibrium solutions in the Earth-Moon BCR4BP

PROPERTIES OF THE HAMILTONIAN

Given that the BCR4BP does not represent a conservative system, the Hamiltonian varies along a trajectory and describes the evolution of the energy. This variation in energy is due to the relative position of the spacecraft with respect to the time-dependent primary body(s). The Hamiltonian corresponds to a pseudo-potential function that is derived relative to the Earth-Moon CR3BP. By removing the influence of the Sun, the Hamiltonian reduces to the Jacobi Constant in the Earth-Moon CR3BP. Therefore, in close proximity to the Earth and Moon, the Hamiltonian remains fairly constant, with minor variations due to solar perturbations. As the spacecraft passes further from the Earth-Moon system, the Hamiltonian experiences large variations as the Sun's perturbative force increases. These variations are expressed explicitly as the time derivative of the Hamiltonian, that is,

$$\dot{H}_{EM} = 2nm_4a_4 \left(-x' \sin \theta_s + y' \cos \theta_s \right) \left(\frac{1}{r_{43}^3} - \frac{1}{a_4^3} \right) \quad (7)$$

where n represents the nondimensional mean motion of Sun about the Earth-Moon system. Noting that Equation (7) is only dependent on the position of the spacecraft and the orientation of the Sun, \dot{H}_{EM} is strictly a function of the spacecraft position in the Sun- B_1 rotating frame. A heat map is plotted in Figure 4, illustrating the evolution of the Hamiltonian in the Earth-Moon-Sun BCR4BP as a function of position in the Sun- B_1 rotating frame. The regions are separated by the y -axis and the curve $r_{43} = a_4$. In close proximity to the Earth-Moon system, the regions of space are separated into four distinct quadrants of the Sun- B_1 rotating frame, centered at B_1 . Previous studies have investigated the tidal impacts on a spacecraft within the vicinity of P_2 .¹⁵ Within the CR3BP, the tidal influence caused by P_1 impacts the periapse and eccentricity of an orbit in close proximity to P_2 . For this analysis, the evolution of the Hamiltonian value is related to those four quadrants.

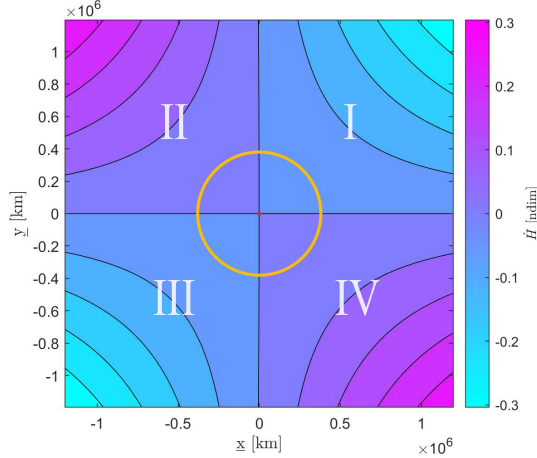


Figure 4. Contour plot illustrating the value of \dot{H}_{EM} at various locations throughout the Sun- B_1 rotating reference frame centered at B_1 with the Sun to the left (yellow circle represents the Moon's orbit)

Ballistic lunar transfers require a high launch energy, corresponding to a low Hamiltonian value. To minimize propellant requirements, a successful ballistic lunar transfer arrives at the Moon with an energy level near to that of the destination orbit energy. For most desired destinations, the Hamiltonian of the arrival orbit near the Moon is greater than the initial Hamiltonian at trans-lunar injection. Thus, when ballistic lunar transfers are constructed, the paths commonly traverse quadrants two and four in Figure 4. In these quadrants, the Sun decreases the spacecraft energy (raises the Hamiltonian) prior to arrival in the vicinity of the Moon and aids in the characterization of transfer structures. The change in the Hamiltonian characterizes the perturbing influence of the Sun on the spacecraft's path. The trajectory plotted in blue in Figure 5a is an example of a ballistic lunar transfer plotted in the Sun- B_1 rotating coordinate frame, where the yellow circle is the lunar orbit; Figure 5b displays the corresponding Hamiltonian value along the transfer over time, where the colored points along the arc correspond to the same state as the colored points in Figure 5a. By comparing the ballistic lunar transfer to the variation in the Hamiltonian, the transfer experiences the largest change in energy when travelling far from the Earth-Moon system in the proper quadrant (denoted by the purple point).

A similar procedure is followed for time history of the Sun- B_1 Hamiltonian. Both models represent the Earth-Moon-Sun system, whether represented in terms of the P_1-P_2 or P_4-B_1 reference frames. The difference arises in the formulation of the pseudo-potential function for a representation within the context; of a given rotating reference frame. The P_4-B_1 model represents the Sun

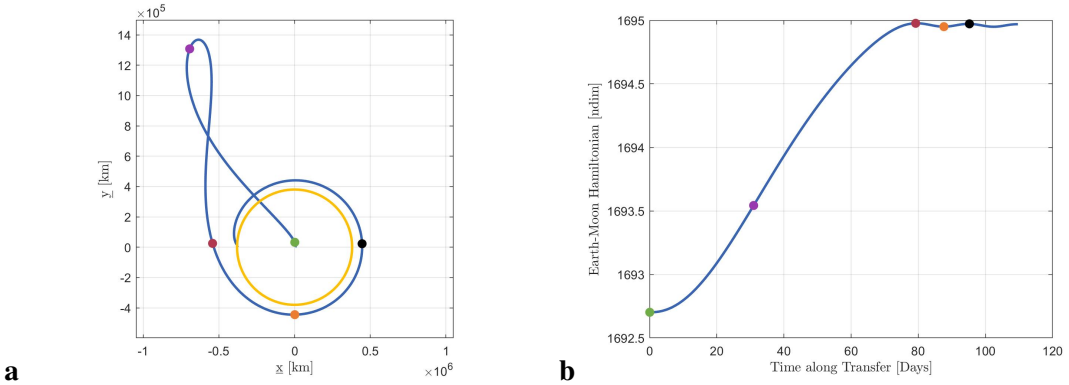


Figure 5. A ballistic lunar transfer in the Sun- B_1 rotating coordinate frame, centered at B_1 with the Sun to the left (a); the corresponding Earth-Moon Hamiltonian vs time for the transfer (b)

and B_1 in fixed positions, where the Sun- B_1 Hamiltonian is expressed as,

$$H_{SB_1} = 2\underline{\Upsilon} - \underline{V}^2 \quad (8)$$

Then, $\underline{V}^2 = \dot{x}^2 + \dot{y}^2 + \dot{z}^2$, recalling that \underline{x} , \underline{y} , and \underline{z} are position components of P_3 relative to B_2 in the Sun- B_1 rotating coordinate frame, $\dot{\underline{x}}$, $\dot{\underline{y}}$, and $\dot{\underline{z}}$ are the relative velocity components of P_3 in the Sun- B_1 rotating coordinate frame, and $\underline{\Upsilon}$ is the Sun- B_1 pseudo-potential function defined as,

$$\underline{\Upsilon} = \frac{1}{2} \left(\underline{x}^2 + \underline{y}^2 \right) + \frac{1 - \underline{\mu}}{r_{43}} + \frac{\underline{\mu}(1 - \underline{\mu})}{r_{13}} + \frac{\underline{\mu}\underline{\mu}}{r_{23}} \quad (9)$$

where the value $\underline{\mu}$ represents the mass parameter in the Sun- B_1 system, $\underline{\mu} = \frac{M_4}{M_1 + M_2 + M_4}$. The derivative of Sun- B_1 Hamiltonian with respect to nondimensional time reflects perturbations due to the alignment of the Earth and Moon, explicitly written as,

$$\dot{H}_{SB_1} = -2n \left((1 - \underline{\mu} - \underline{x}) \sin \theta_{EM} + \underline{y} \cos \theta_{EM} \right) \left(\frac{1}{r_{23}^3} - \frac{1}{r_{13}^3} \right) \quad (10)$$

From Figure 2b, observe that θ_{EM} describes the angle of the Earth-Moon line relative to the Sun- B_1 line, and it is related to the Sun angle such that $\theta_{EM} = \pi - \theta_S$. The time derivative of the Sun- B_1 Hamiltonian, \dot{H}_{SB_1} , is a function solely of the system parameters and the spacecraft position in the Earth-Moon rotating frame, independent of the position of the Sun. Take a model where the Earth and Moon are simplified to a single point mass at the location of B_1 , the problem then becomes equivalent to the Sun- B_1 CR3BP, where the Sun- B_1 Hamiltonian becomes an integral of the motion, i.e., the Jacobi Constant. Thus, the motion of the Earth-Moon system acts as the perturbative force in the formulation relative to the Sun- B_1 rotating coordinate frame. Figure 2b provides a visual representation for the evolution of the primary bodies P_1 and P_2 throughout time in the Sun- B_1 rotating frame. A contour plot in Figure 6 depicts the variations of \dot{H}_{SB_1} as P_3 passes through the various quadrants in the Earth-Moon rotating frame. As \dot{H}_{EM} and \dot{H}_{SB_1} are formulated in two different frames, their nondimensional energy rate of change are not related to one another, thus, a direct comparison between the values expressed in Figure 4 and Figure 6 is not useful. The quadrants reflecting the rates of change of the Hamiltonian, i.e., \dot{H}_{SB_1} , in Figure 6 are not as uniform as they appear in the figure. Regions with the largest magnitudes of \dot{H}_{SB_1}

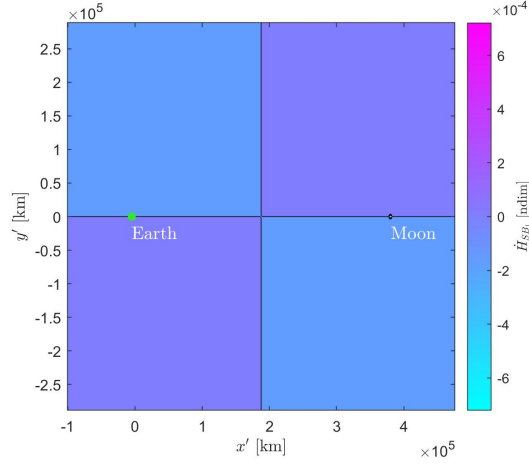


Figure 6. Contour plot illustrating the value of \dot{H}_{SB_1} in each quadrant throughout the Earth-Moon rotating reference frame

in Figure 6 occur near the Earth and Moon. To further visualize these energy surfaces, Figure 7 illustrates \dot{H}_{SB_1} in the vicinity of both the Earth and Moon. In Figure 7, the Earth and Moon are depicted as green and gray circles, respectively. For regions off of the x' -axis, i.e., $|y'| > 0$, the magnitude of \dot{H}_{SB_1} increases as the distance to either of the primaries decreases. For locations along the x' -axis and equidistant from either the Earth and Moon, the magnitude of \dot{H}_{SB_1} is zero. Recall that a decrease in the Hamiltonian value correlates to an increase in the spacecraft energy. For ballistic lunar transfers, the Sun- B_1 Hamiltonian provides insight into the path of the spacecraft as it initially departs the Earth-Moon region. To increase the outbound energy of the spacecraft, i.e., lower the ΔV required at trans-lunar injection, either lunar and/or Earth flybys offer opportunities. To produce the desired change in H_{SB_1} , a spacecraft encounters the Earth on the positive half of y' -axis in the Earth-Moon rotating frame or encounter the Moon in the quadrant such that $y' < 0$ in the Earth-Moon rotating frame, such that \dot{H}_{SB_1} decreases. Understanding the rates of change of the Hamiltonian provides insight into natural structures which govern the energy of a spacecraft.

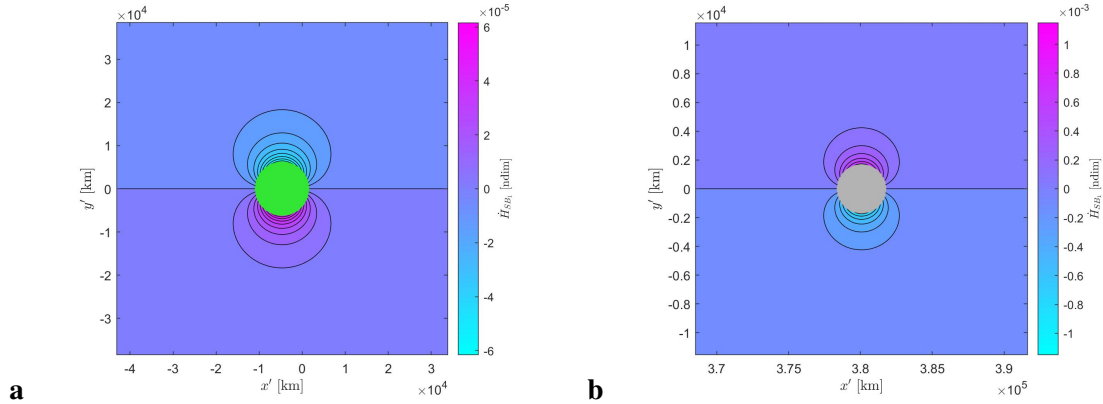


Figure 7. Contour plots illustrating the value of \dot{H}_{SB_1} in proximity to the Earth in green (a), and Moon in gray (b) in the Earth-Moon rotating coordinate frame

CONSTRUCTING BALLISTIC LUNAR TRANSFERS IN THE CR3BP

To construct a successful ballistic lunar transfer, the overall transfer geometry and the arrival conditions at the Moon are most significant. Dynamical structures available in the Earth-Moon and Sun-Earth CR3BP systems can be examined independently. To identify advantageous locations in the vicinity of the Moon, the Earth-Moon CR3BP provides a sufficient representation of the dynamical environment for preliminary design. Additionally, construction of instantaneous equilibrium solutions and periodic orbits in the BCR4BP is seeded via initial guesses from solutions in the Earth-Moon CR3BP.¹⁶ The Sun-Earth CR3BP model is beneficial in modeling the influence of solar perturbations on the spacecraft as it departs the Earth-Moon region. The Sun-Earth CR3BP is explored in this investigation to construct families of ballistic lunar transfer geometries and to characterize their energy evolution and time of flight.

Poincaré maps are an effective tool to aid in characterizing the structures in a dynamical system. In this investigation, periapse Poincaré maps are leveraged. These maps represent discrete points in configuration space where a periapse occurs. The efficacy of periapse Poincaré maps are dependent on the initial conditions used to generate the map. For this analysis, initial conditions are selected along the arrival or departure orbit in position space, which ties the information from the map back to those originating locations. Consider the Sun-Earth CR3BP where a periapse map is constructed by discretizing points on the xy -plane in the Sun-Earth rotating frame along a circular parking orbit about the Earth and, for each point along the orbit, a ΔV is applied in the velocity direction. The ΔV is constructed by constraining the magnitude of the velocity for the post maneuver states to match in all Jacobi Constant values; the trajectories are then propagated forward for 365 days in the Sun-Earth CR3BP.¹⁷ Consider the periapse map in Figure 8a where the initial conditions are distributed in a 150 km altitude Earth parking orbit and a ΔV is applied to achieve a Jacobi Constant of $C = 3.000804$. The ΔV vector is applied along the velocity direction in the rotating coordinate frame. A representation of the Moon orbit is also plotted on the map in gold. The purple dot in Figure 8a represents a perigee point that occurs at the lunar orbit radius and the transfer trajectory associated with that point is plotted in Figure 8b. This transfer, identified from the perigee point on the Poincaré map, supplies a sufficient initial guess to be transitioned to either the BCR4BP or to an ephemeris model.

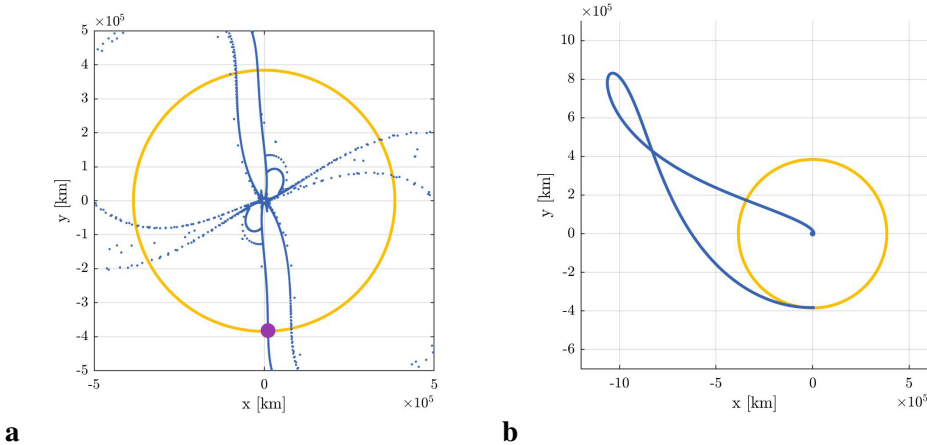


Figure 8. Periapse Poincaré Map ($C = 3.000804$) in Sun-Earth CR3BP (a); trajectory associated with purple periapse point in the Sun-Earth Rotating Frame (b)

The insight provided by a periapse Poincaré map in the CR3BP is related to the Jacobi Constant value. The periapse map in Figure 8a offers detail on a trajectory that departs from the Earth and arrives at the lunar orbit radius for a specified energy. A similar analysis completed for a new pair of Jacobi Constant values depicts the evolution of transfers across two different energy levels. Using the same initial positions from Figure 8a, the two periapse maps in Figure 9 illustrates the progression of accessible transfers as the Jacobi Constant decreases. The map in Figure 9a is constructed for a Jacobi Constant value of $C = 3.000854$, where the energy is insufficient to allow the periapse to reach the lunar orbit radius. When the Jacobi Constant is reduced to a value of $C = 3.000829$, the downstream perigee distances for the transfers reach the altitude of the lunar orbit radius, as observed in Figure 9b. Comparing Figures 8a and 9b, the points on each map possess a Jacobi Constant value that allow the perigees to reach a particular altitude; however, the higher energy map (lower Jacobi Constant) includes more perigees located at the lunar orbit radius.

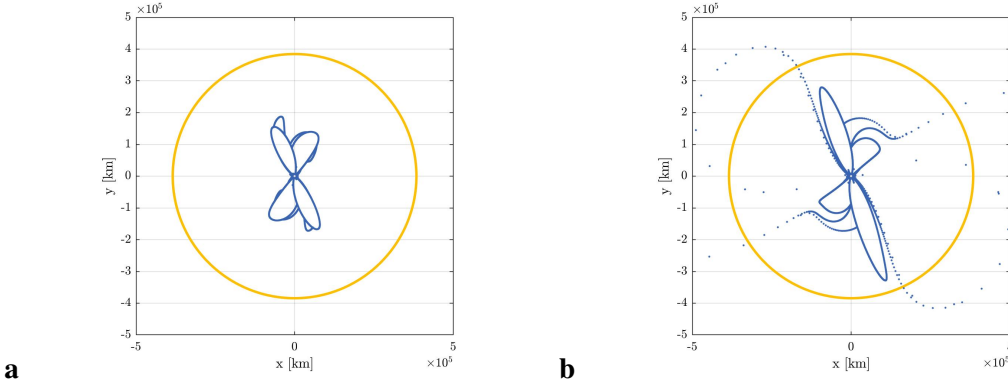


Figure 9. Periapse Poincaré Maps in the Sun-Earth CR3BP each for a specific value of the Jacobi Constant, $C = 3.000854$ (a); $C = 3.000829$ (b)

To expand to a range of solutions and deliver a broader set of transfer characteristics, a suitable continuation strategy is effective. A continuation scheme is seeded with an initial guess from a periapse map and families of ballistic lunar transfers are computed in the CR3BP. By constraining the initial state to be located at a 150 km altitude Earth perigee and constraining the final state as perigee with a radius equal to the lunar orbit radius, a family of solutions is generated such that the Jacobi Constant value and time of flight vary across each member of the family. Using the transfer in Figure 8b as an initial guess, a family of ballistic lunar transfers is computed and plotted in Figure 10a. Not constrained by energy, the full family contains transfers that traverse a significant region of the Sun-Earth system and pass through multiple quadrants. The times of flight continue to increase in both directions from the original transfer. The gray transfers plotted in Figure 10a represent a subset of the family with a time of flight shorter than 130 days, and shift towards quadrant II in the Sun-Earth rotating coordinate frame. This subset remains in relatively close proximity to Earth, and includes the transfers with the minimum energy (yellow) and shortest time of flight (green) along the family of transfers. The transfer with the maximum Jacobi Constant has a value of $C = 3.0008264$ and a time of flight of 97.7 days. The transfer with the shortest time of flight has a duration of 75.9 days, and a Jacobi Constant value of $C = 3.0007286$. The curve in Figure 10b depicts the evolution of the Jacobi Constant and time of flight across the family.

One advantage to the family in Figure 10a is that the shorter times of flight relative to other ballistic lunar transfer geometries. Many families of ballistic lunar transfers exist in the Sun-Earth CR3BP. By selecting other initial conditions from the periapse Poincaré map in Figure 9b, additional

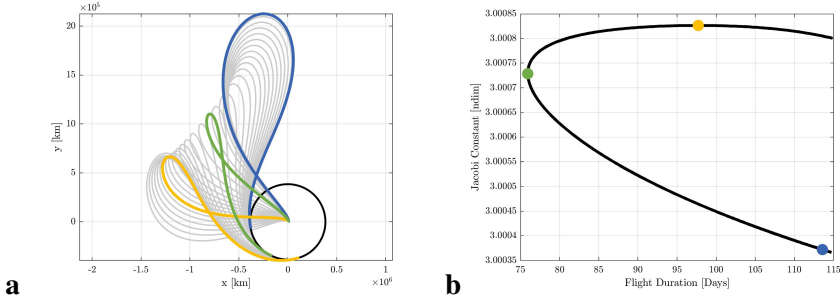


Figure 10. Family 1: Family of ballistic lunar transfers in the CR3BP approaching L₁ (a); the corresponding Jacobi Constant vs time of flight for the transfers (b)

families of ballistic lunar transfers are also straightforwardly constructed. Figures 11-13 display families with three different geometries. Each figure includes the evolution of the Jacobi Constant and time of flight for each member of the family. In Figure 11a, consider the green transfer geometry described Earth to Earth to Moon. Where the initial Earth to Earth arc departs from the initial perigee condition, and performs another perigee close to Earth prior to arrival at the lunar orbit radius. Yet a different family is plotted in Figure 12. The transfers in Figure 12a remain in near-heliocentric space for a longer interval, prior to arrival at the lunar orbit radius. All three families plotted in Figures 10a-12a demonstrate an initial departure from the Earth towards the Sun, or directed toward quadrant II. Each family is related to a corresponding family that departs towards quadrant IV. One such example appears in Figure 13a where blue, green, and yellow transfers representing behaviour similar to the motion in 10a, except that the family members traverse away from the Sun initially. Although the curves in Figures 10b and 13b appear the same, the motion toward quadrant II results in a slightly lower energy and time of flight.

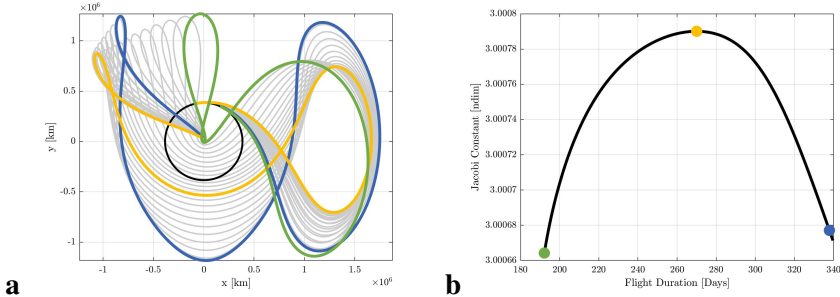


Figure 11. Family 2: Family of ballistic lunar transfers in the CR3BP (a); the corresponding Jacobi Constant vs time of flight for the transfers (b)

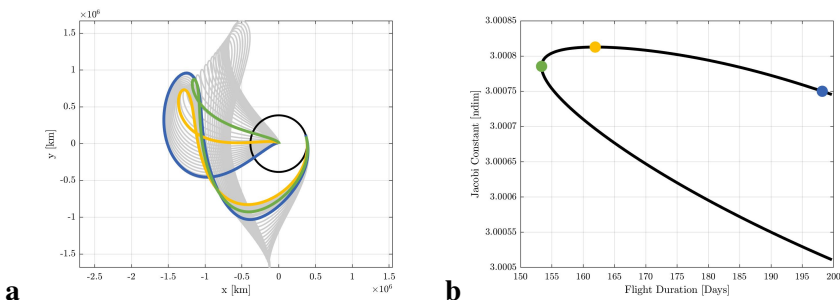


Figure 12. Family 3: Family of ballistic lunar transfers in the CR3BP approaching L₁ (a); the corresponding Jacobi Constant vs time of flight for the transfers (b)

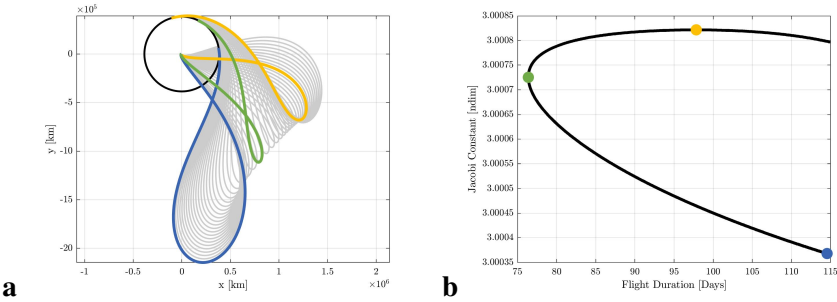


Figure 13. Family 4: Family of ballistic lunar transfers in the CR3BP approaching L₂ (a); the corresponding Jacobi Constant vs time of flight for the transfers (b)

CONSTRUCTING BALLISTIC LUNAR TRANSFERS IN THE BCR4BP

As ballistic lunar transfers are defined by the gravitational influences of the Earth, Moon, and Sun, the BCR4BP is an effective model for constructing these transfers. The dynamical structures within the four-body model flow back and forth between the dominant influence of the Sun- B_1 and Earth-Moon systems while following a truly ballistic path. The model is advantageous as manifold structures associated with periodic solutions are employed to produce low energy solutions. In addition, the assumptions in the BCR4BP also deliver transfer geometries that are repeatable each synodic month. This investigation is currently focused on ballistic lunar transfers to conic orbits and libration point orbits about the Moon in the planar problem. Two different approaches are examined to produce ballistic lunar transfers. The first strategy incorporates dynamical structures from both the CR3BP and BCR4BP as an initial guess to traverse from a low Earth orbit to a low lunar orbit. A second technique leverages transfers to planar libration point orbits, utilizing manifolds structures, small insertion maneuvers, and periapse Poincaré maps.

Ballistic Lunar Transfers to Conic Orbits

One approach to computing ballistic lunar transfers in the BCR4BP is by leveraging an initial guess from the CR3BP. As noted previously, there are several transfer geometries available in the Sun-Earth system, and selecting an initial guess is dependent on the specific mission constraints. The process of constructing families of ballistic lunar transfers in the BCR4BP is dependent on the initial guess. Using an initial guess trajectory, similar to the trajectory illustrated in Figure 8b, a family of solutions is produced in the BCR4BP. By constraining the initial state to be located at a 150 km altitude perigee and constraining the final state to arrive at a 100 km perilune in the $x' - y'$ -plane of the Earth-Moon rotating frame, a family of solutions is generated such that Sun-Moon-Earth orientation is constant upon arrival in the lunar vicinity. The corrections process employed in this analysis is conducted within the Earth-Moon rotating frame. The resulting family of solutions is plotted in Figure 14a, along with a plot of the insertion ΔV for each transfer to circularize the orbit around the Moon as a function of time of flight (Figure 14b). The colored points in Figure 14b correspond to the same colored transfers along the family plotted on Figure 14a. Note that the minimum ΔV solution for this family is highlighted in blue in Figure 14a. An initial guess from the Sun-Earth CR3BP supplies a sufficient initial guess for transitioning to the BCR4BP and seeds a continuation scheme to construct a family of solutions.

Selecting another member of the family plotted in Figure 10a, one associated with a different Sun angle upon arrival at the Moon, a family is constructed by constraining the arrival Sun angle at the Moon. The transfer is selected to approach the vicinity of the Moon upon departure from the

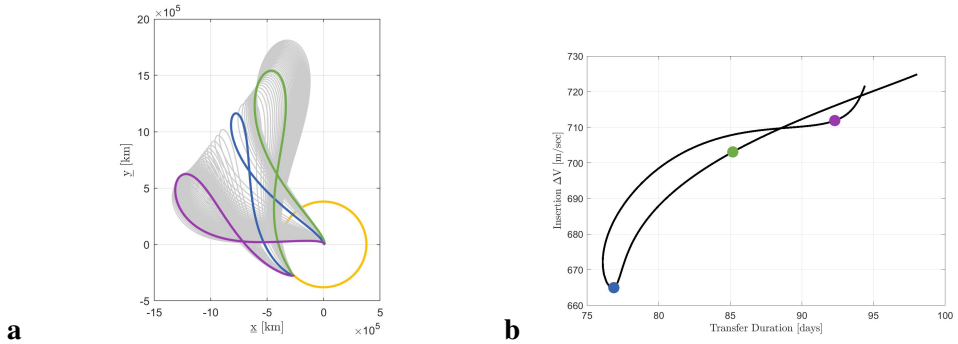


Figure 14. Family of ballistic lunar transfers in the BCR4BP expressed in the Sun- B_1 rotating frame (a); the corresponding lunar circularization ΔV vs time of flight for the family of BLTs (b)

Earth-Moon system. Figure 15 illustrates a family of transfers from the 150 km circular low Earth orbit to the 100 km circular low lunar orbit, where select members of the family include lunar flybys that significantly alter the path of the outbound leg of the trajectory. The plots in Figures 16a and 16b represent the trans-lunar injection ΔV and the lunar orbit insertion (LOI) maneuver ΔV for the family of transfers, respectively. One example of a trajectory that encounters the Moon is illustrated in blue in Figure 15, and is plotted as a blue dot in Figures 16a and 16b. For ballistic lunar transfers, an outbound lunar or Earth encounter reduces the initial cost of departing the Earth-Moon system, i.e., the trans-lunar injection burn. For the examples introduced here an outbound lunar flyby results in a savings of approximately 80 m/s while maintaining the same time of flight.

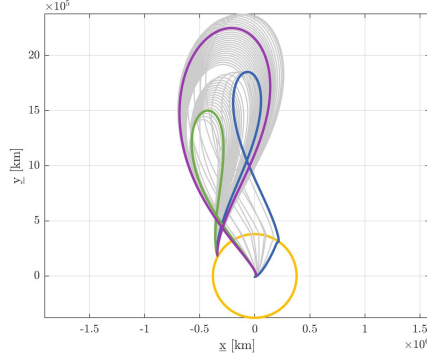


Figure 15. Family of ballistic lunar transfers in the BCR4BP expressed in the Sun- B_1 rotating frame, the colored transfers correspond to the plots in Figure 16

Families of ballistic lunar transfers with fixed times of flight are constructed following the same procedure, but the time of flight is constrained rather than the Sun-Earth-Moon orientation upon arrival. Since the orientation of the Earth-Moon-Sun system is periodic, the family departs from the Earth and arrives near the Moon covering all ranges of Sun angles θ_s between 0 and 360 degrees. The fixed time of flight family is plotted in the Sun- B_1 frame in Figure 17a, where each member of the family possesses a 73-day time of flight. Figure 17b illustrates the evolution of the insertion ΔV across all Sun angles; the colored dots on the curve represent the trajectories with the corresponding departure Sun angles and insertion ΔV s as rendered in Figure 17a with the equivalent color. The progression of the family differs from the ballistic lunar transfers previously produced in this investigation. Transfers that depart towards quadrants II and IV, plotted in blue and green, remain similar to the geometry that appears in Figures 10a, 13a, and 14.

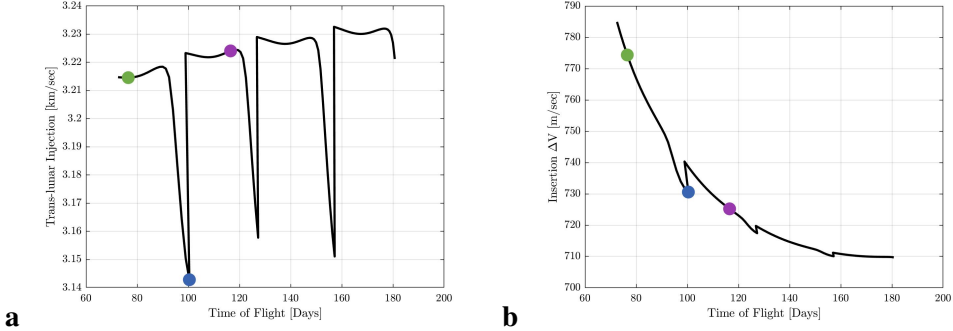


Figure 16. Plots showcasing the trans-lunar injection (a) and lunar orbit insertion (b) maneuver costs for the family of ballistic lunar transfers in Figure 15

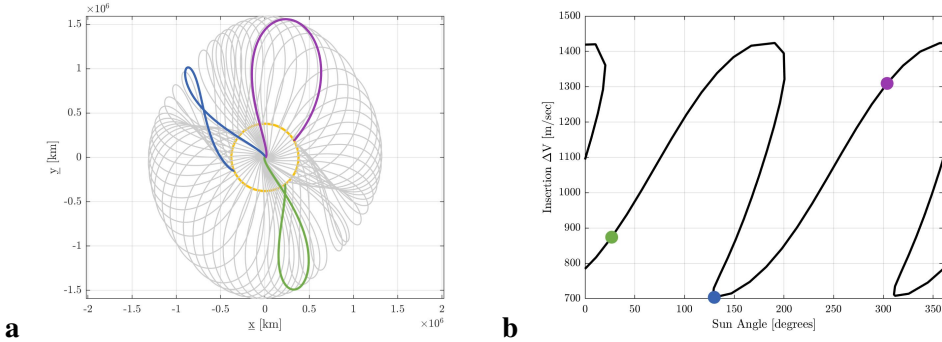


Figure 17. Family of ballistic lunar transfers in the BCR4BP expressed in the Sun- B_1 rotating frame (a); the corresponding lunar circularization ΔV vs departure Sun angle for the family of BLTs (b)

Families of ballistic lunar transfers are also constructed using the instantaneous equilibrium solutions in the BCR4BP. As the instantaneous equilibrium solutions are dependent on the orientation of the Earth-Moon-Sun system, the points represent trajectories that explore the entire system. By leveraging trajectories computed using the instantaneous equilibrium solutions at E_2 , paths depart the lunar vicinity corresponding to the highest Hamiltonian value that permits traversal through Earth-Moon L_2 portal. Thus, for mission profiles that insert directly into a low lunar orbit, this approach offers the theoretical minimum energy level for insertion into such a destination orbit. To construct the family of ballistic lunar transfers, an initial guess is supplied from a trajectory propagated from an instantaneous E_2 point. A set of E_2 points propagated forward and backward must meet two conditions. The forward propagated segment from the E_2 points must achieve a perilune prior to departing the lunar vicinity. The location of this perilune is the insertion point onto a sample circular lunar orbit. Fulfilment of the second condition requires achieving a low altitude perigee when the same E_2 point is propagated backwards in time. By analyzing a dense set of instantaneous E_2 points, only a small subset of the instantaneous equilibrium solutions meet both conditions. One example of a transfer that meets both conditions is plotted in Figure 18.

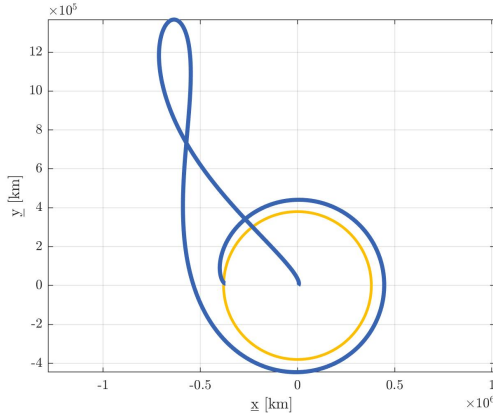


Figure 18. One trajectory from the E_2 instantaneous equilibrium solutions that has ballistic lunar transfers behaviour, and has a perilune in close proximity to the Moon, plotted in Sun-B₁ rotating frame

The transfer accomplished a time of flight of 109 days, and reaches a lunar orbit altitude at 7200 km above the surface of the Moon. As various missions consider destination orbits at a lower altitudes at the Moon, it is beneficial to explore transfers that arrive with a lower perilune altitude. Using the trajectory from Figure 18 as an initial condition, a family of ballistic lunar transfers is constructed by decreasing the arrival altitude at the Moon. Each member of the resulting family is constrained to possess a departing perigee altitude of 150 km at the Earth, and arrive at the Moon as a perilune; the altitude of the perilune varies across members of the family. Figure 19a illustrates the family of ballistic lunar transfers in the Earth-Moon rotating coordinate frame as they approach the Moon. The curve in Figure 19b depicts the evolution of the circularizing maneuver ΔV as the lunar orbit altitude increases.

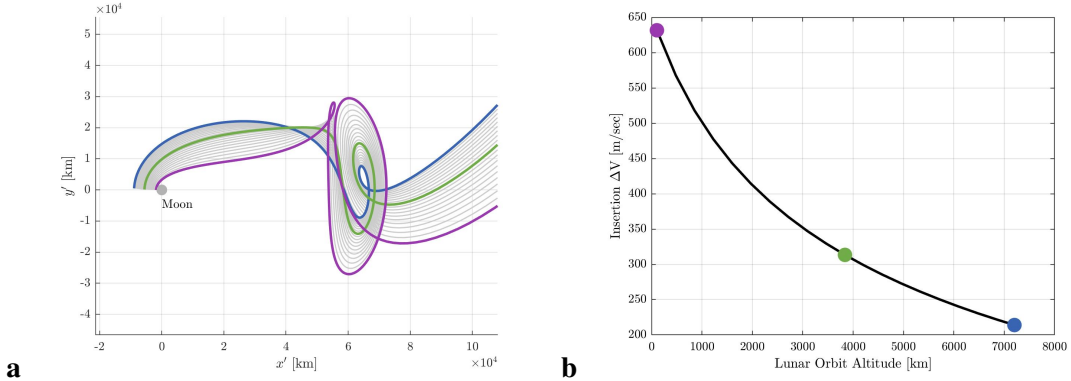


Figure 19. Family of ballistic lunar transfers in the BCR4BP viewed in the Earth-Moon rotating frame centered at the Moon (a); the corresponding lunar circularization ΔV vs lunar orbit altitude for the family of BLTs (b)

Theoretical Minimum ΔV

One challenge associated with the design of ballistic lunar transfers is constructing transfer that possess the minimum LOI ΔV . For truly ballistic transfers, no deterministic maneuvers are required post-trans-lunar injection, however, many destinations require an insertion maneuver upon arrival in the lunar region and arrival constraints may increase the challenge. In this investigation,

the theoretical minimum insertion ΔV is examined. Properties of the BCR4BP are leveraged to characterize the efficiency of a ballistic lunar transfer upon arrival in cislunar space. Consider a spacecraft performing a maneuver at a fixed position and epoch. The change in velocity required is computed using the following,

$$|\Delta V| = \sqrt{V_1^2 + V_2^2 - 2V_1 V_2 \cos \alpha} \quad (11)$$

where $|\Delta V|$ is the magnitude of the change in velocity, V_1 and V_2 represent the initial and final velocity magnitudes respectively, and α is the angle between the two velocity vectors \vec{V}_1 and \vec{V}_2 . For simplicity, assume that the incoming velocity is greater than the final velocity, or $V_1 > V_2$. As the two velocity magnitudes are held constant, determining the minimum ΔV is trivial, i.e., $\alpha = 0$. If it is assumed that the incoming velocity must be parallel to the final velocity direction for the theoretical insertion maneuver, then Equation (11) is simplified to $|\Delta V| = V_1 - V_2$. Similarly, by rearranging Equation (4) as a function of velocity, the minimum ΔV equation is defined,

$$|\Delta V| = \sqrt{2\Upsilon_1 - H_1} - V_2 \quad (12)$$

where Υ_1 represents the initial pseudo-potential function, and H_1 is the Earth-Moon Hamiltonian for the incoming state prior to the maneuver. The minimum ΔV essentially allows solely for the energy change that is required without regard to a non-tangential direction. It is now fully defined by the pre-maneuver position and velocity and the desired final velocity. This relationship is available to provide a metric for comparison of a given maneuver magnitude to the theoretical minimum at any given position.

An energy analysis for the destination orbit is accomplished to compute the theoretical minimum insertion maneuver required at a given arrival state. As the BCR4BP is a non-autonomous system, the Hamiltonian varies significantly depending on the path of the spacecraft. To bound the problem, some assumptions concerning the characteristics of a ballistic lunar transfer are incorporated. First, it is assumed that the transfer transits through the E_2 gateway prior to arrival at the destination orbit. This assumption limits the highest possible incoming Hamiltonian, i.e., the lowest possible energy, for the incoming spacecraft. To represent the minimum ΔV upon insertion, it is also assumed that the incoming Hamiltonian for the ballistic lunar transfer is equal to the maximum Hamiltonian from the set of E_2 instantaneous equilibrium solutions (Figure 3b). Additionally, since the pseudo-potential is a function only of the position and Sun angle, it is also assumed that $\Upsilon_1 = \Upsilon_2$. Using Equation (12) and knowledge of the insertion location along the destination orbit, the theoretical minimum insertion maneuver is evaluated as,

$$|\Delta V_{min}| = \sqrt{2\Upsilon_2 - H_{E_2}} - V_2 \quad (13)$$

where H_{E_2} is the maximum Hamiltonian from the set of E_2 instantaneous equilibrium solutions. For this analysis, the value of $H_{E_2} \approx 1694.973$. Equation (13) is independent of the ballistic lunar transfer conditions, therefore ΔV_{min} is a function of insertion location and the E_2 Hamiltonian. The assumptions do limit the insight from comparison of the cost with ΔV_{min} ; the Hamiltonian value for a ballistic lunar transfer continues to vary after arrival through the E_2 gateway into the lunar vicinity. After a long period of exposure to the dynamics in the Earth-Moon system, small perturbations continue to impact the overall energy of the transfer. Therefore, it is possible to determine solutions with a cost below the value computed in Equation (13) by allowing a longer transit within the vicinity of the Moon prior to insertion, or by implementing multiple maneuvers. However,

ΔV_{min} is simply a metric to compare known ballistic lunar transfers. For example, the theoretical minimum ΔV for insertion into a circular lunar orbit from a ballistic lunar transfer is summarized in Figure 20. As the altitude of the circular orbit increases, the orbital energy approaches the value for H_{E_2} and, thus, the required maneuver magnitude decreases. Consider the ΔV costs for the family of transfers constructed from the instantaneous equilibrium solution as plotted in Figure 19b. The magnitude of the insertion maneuver remains within 2 m/s of the theoretical minimum. For orbits that possess a Hamiltonian value less than H_{E_2} , Equation (13) is a non-physical value and corresponds to insertions that possess a theoretical minimum insertion maneuver magnitude of zero. A destination orbit satisfying this condition possesses Hamiltonian values at locations along specific arcs along the orbit, or even the entire period of the orbit such that the E_2 gateway is open. However, due to stability implications, a true ballistic insertion maybe difficult to achieve for an orbit that is stable or nearly stable. In this scenario, transfers require a longer time of flight or a maneuver to reach the destination orbit.

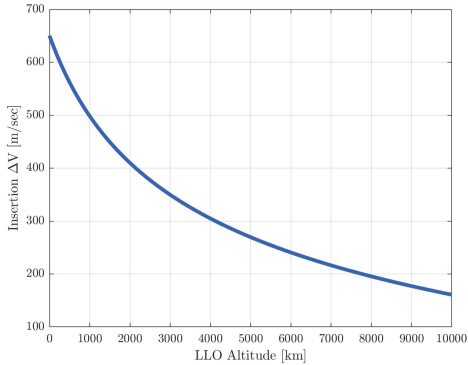


Figure 20. Plot showcasing the theoretical minimum insertion magnitude (ΔV_{min}) required for a ballistic lunar transfer to arrive into a circular low lunar orbit

Ballistic Lunar Transfers to Planar Libration Point Orbits

Dynamical systems theory is leveraged to compute ballistic lunar transfers to libration point orbits. Libration point orbits serve as both intermediate and destination orbits to explore the lunar vicinity due to their high energy compared to low lunar orbits. Additionally, unstable libration point orbits provide insight into the natural flow through cislunar space. Examples of planar, unstable orbit families in the CR3BP are the L_1 and L_2 Lyapunov orbits. Members of these families that possess an orbital period equal to the lunar synodic period are straightforwardly transitioned to periodic orbits in the BCR4BP.¹⁸ For the periodic orbits examined in this investigation, the stability properties are consistent between the CR3BP and the BCR4BP. Manifolds structures associated with Lyapunov orbits flow into and out of the lunar vicinity in the BCR4BP. These manifold structures are exploited to aid in construction of ballistic lunar transfers.

Poincaré maps are also leveraged directly in the BCR4BP to determine low energy transfers to the lunar region. Consider a periodic 2:1 synodic resonant Earth-Moon L_2 Lyapunov orbit in the BCR4BP. By propagating the stable manifold trajectories in reverse time, a periapse map is generated and plotted in Figure 21. The periapse number, colored from 1 to 5, is displayed and represents the number of Earth periapses that a specific trajectory experiences prior to arrival on the Lyapunov orbit on the far side of the Moon. Since there are two frames of significance within the Sun-Earth-Moon BCR4BP, the Poincaré map is represented in both the Earth-Moon and Sun- B_1

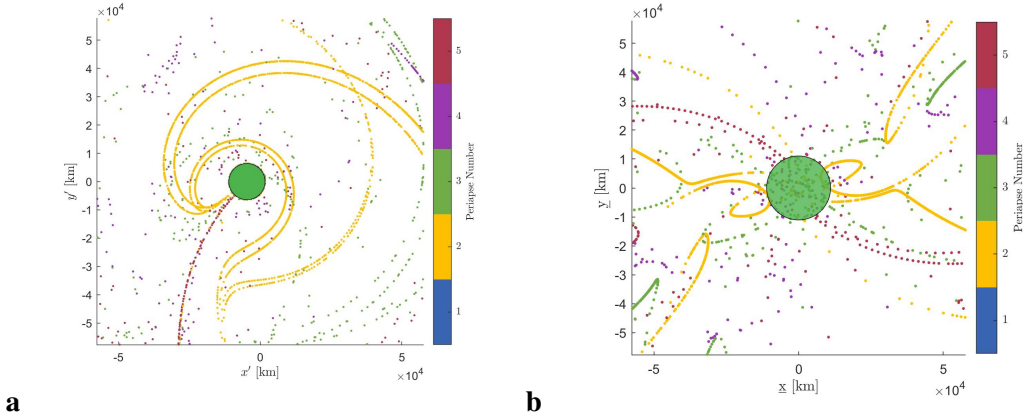


Figure 21. Periapse Poincaré Maps in the Sun-Earth-Moon BCR4BP using manifolds off the 2:1 L₂ Earth-Moon Lyapunov, plotted in the Earth-Moon (a) and Sun-B₁ (b) rotating frames. The green disk represents the fixed position of the Earth in the Earth-Moon frame (a), and the region of space the Earth encompasses as it moves throughout the Sun-B₁ frame (b)

rotating frames. Examining the periapses and their history in both frames reveals structures relative to the alignment of the systems. Selecting a trajectory associated with a periapsis point near a low Earth altitude from either map in Figure 21 provides a maneuver-free transfer trajectory originating near the Earth to the 2:1 L₂ Lyapunov orbit. Periapse Poincaré maps also offer insight into the various transfer geometries available. The location of the points on the map illustrate the periapse locations relative to the Earth, the color scale in Figure 21 expresses the number of revolutions around the Earth prior to arrival in the 2:1 L₂ Lyapunov orbit. However, other characteristics such as the initial Hamiltonian value and the time of flight are also used to uncover solutions that satisfy specific mission criteria. The periapse with a maximum initial Hamiltonian value is selected in Figure 21a and the respective transfer trajectory is displayed in Figures 22a and 22b, where the green arc represents the arrival in 2:1 L₂ Lyapunov orbit in both the Sun-B₁ and Earth-Moon rotating frames respectively. The yellow circle in Figure 22a represents the lunar orbit. The flight duration for the transfer is approximately 153 days, and departs from the surface of Earth with a $\Delta V = 3.188$ km/s. The path includes an outbound lunar flyby at an altitude of 2700 km. The dynamics of the transfer upon arrival at in the lunar vicinity is apparent in Figure 22b, where the Moon is rendered in grey.

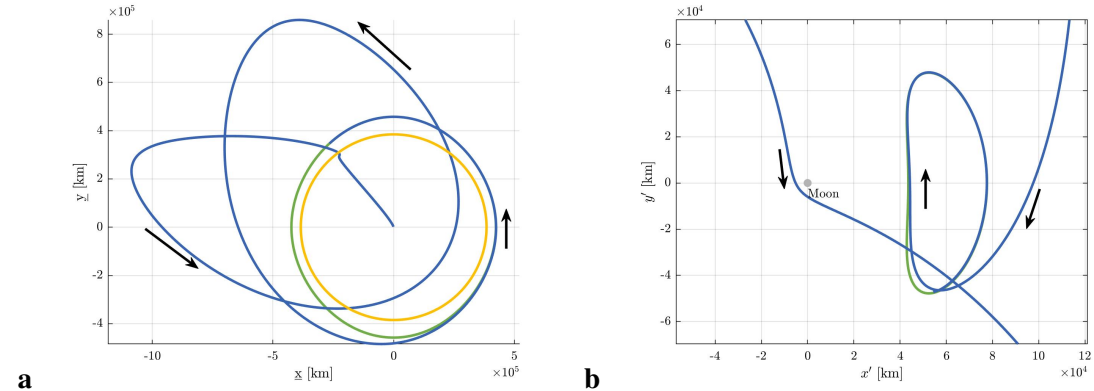


Figure 22. Ballistic lunar transfer with an outbound lunar flyby (blue) to a 2:1 synodic resonant L₂ Lyapunov Orbit (green), plotted in the Sun-B₁ (a) and Earth-Moon (b) rotating frames.

Stable libration point orbits are also advantageous for mission operations as spacecraft remain within these orbits with minimal station keeping maneuvers. However, stable and unstable manifold structures to these stable libration point orbits do not exist. Periapse Poincaré maps are again leveraged to construct ballistic lunar transfers to such linearly stable orbits. Consider a 3:1 lunar synodic Earth-Moon distant retrograde orbit (DRO). Periapse Poincaré maps are constructed by discretizing points along the DRO, imparting a ΔV vector parallel to the state velocity vector and propagating the state in reverse time. Not surprisingly, the magnitude of the maneuver impacts the geometry of the resultant transfers. For low ΔV magnitudes, trajectories remain in the vicinity of the Moon for months prior departing the lunar vicinity in reverse time. For larger ΔV magnitudes, time in the lunar vicinity before arrival in the DRO is reduced. A family of ballistic lunar transfer into a 3:1 synodic resonant DRO is plotted in Figures 23a and 23b. The blue transfer is delivered in a time of flight equal to 100 days, and an insertion maneuver onto the DRO of 75 m/s, the red arc represents the 3:1 synodic resonant DRO in both the Sun- B_1 and Earth-Moon reference frames. Figure 23b illustrates the paths of the family members upon arrival in the lunar vicinity; the transfers complete one half revolution around the Moon prior to insertion onto the DRO. While maneuver size determines the time interval the trajectories remain in the lunar vicinity before insertion, this example ballistic lunar transfer to stable orbits are simply constructed in the BCR4BP using periapse maps.

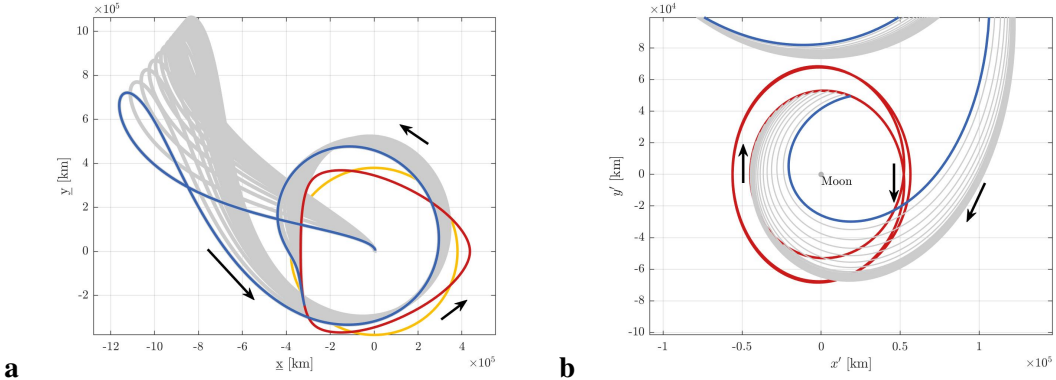


Figure 23. Family of ballistic lunar transfers to a 3:1 synodic resonant Distant Retrograde Orbit, plotted in the Sun- B_1 (a) and Earth-Moon (b) rotating frames.

CONCLUDING REMARKS

Families of ballistic lunar transfers are constructed by leveraging dynamical systems theory. In the Sun-Earth CR3BP, the outbound geometry of a trajectory is apparent as it traverses near-heliocentric space; families represent the fundamental structures for ballistic lunar transfers under a solar perturbing force. By leveraging the Earth-Moon-Sun BCR4BP, the entire motion of a ballistic lunar transfer is captured in a simplified model. Families of transfers leverage the variation in energy upon departure from the Earth-Moon system through lunar and Earth flybys to lower the trans-lunar injection cost. While traversing quadrants II and IV in the Sun- B_1 rotating coordinate frame, the Hamiltonian value for a ballistic lunar transfer increases to assist in lowering the lunar orbit insertion costs. Techniques using periapse Poincaré maps are demonstrated to construct transfers to unstable periodic orbits using manifold structure and stable periodic orbits given an insertion maneuver magnitude. Families of ballistic lunar transfers are constructed by leveraging the dynamical structures associated with the desired destination orbits.

ACKNOWLEDGMENT

The authors would like to thank NSF Grant No. 10001485, the Purdue University School of Aeronautics and Astronautics, and the Rune and Barbara Eliasen Visualization Laboratory for facilities and financial support. The authors would also like to thank the Purdue Multi-Body Dynamics Research Group for insightful discussions.

REFERENCES

- [1] R. M. Smith, N. Merancy, and J. Krezel, “Exploration Missions 1, 2, and Beyond: First Steps Toward a Sustainable Human Presence at the Moon,” *2019 IEEE Aerospace Conference*, Vol. 2019-, IEEE, 2019, pp. 1–12.
- [2] C. Warner, “NASA Outlines Lunar Surface Sustainability Concept,” *web*, Apr. 2020. <https://www.nasa.gov/feature/nasa-outlines-lunar-surface-sustainability-concept>.
- [3] R. Roncoli and K. Fujii, “Mission Design Overview for the Gravity Recovery and Interior Laboratory (GRAIL) Mission,” *American Institute of Aeronautics and Astronautics. AIAA Conference Papers*, Reston, 2010.
- [4] E. A. Belbruno and J. K. Miller, “Sun-perturbed Earth-to-moon transfers with ballistic capture,” *Journal of Guidance, Control, and Dynamics*, Vol. 16, No. 4, 1993, pp. 770–775.
- [5] R. J. Whitley, D. C. Davis, L. M. Burke, B. P. McCarthy, R. J. Power, M. L. McGuire, and K. C. Howell, “Earth-Moon Near Rectilinear Halo and Butterfly Orbits for Lunar Surface Exploration,” *AIAA/AAS Astrodynamics Specialist Conference*, 2018.
- [6] J. S. Parker and G. H. Born, “Modeling a Low-Energy Ballistic Lunar Transfer Using Dynamical Systems Theory,” Vol. 45, 2008, pp. 1269–1281.
- [7] J. S. Parker, “Targeting Low-Energy Ballistic Lunar Transfers,” *The Journal of the Astronautical Sciences*, Vol. 58, No. 3, 2011, pp. 311–334.
- [8] N. L. Parrish, E. Kayser, S. Udupa, J. S. Parker, B. W. Cheetham, and D. C. Davis, “Ballistic Lunar Transfers to Near Rectilinear Halo Orbit: Operational Considerations,” *AIAA Scitech 2020 Forum*.
- [9] K. Oshima, F. Topputo, and T. Yanao, “Low-energy Transfers to the Moon with Long Transfer Time,” *Celestial Mechanics and Dynamical Astronomy*, Vol. 131, No. 1, 2019, pp. 1–19.
- [10] K. C. Howell, D. C. Davis, and A. F. Haapala, “Application of Periapse Maps for the Design of Trajectories near the Smaller Primary in Multi-body Regimes,” *Mathematical Problems in Engineering*, Vol. 2012, No. 2012, 2012.
- [11] D. C. Davis and K. C. Howell, “Characterization of Trajectories Near the Smaller Primary in the Restricted Problem for Applications,” *Journal of Guidance, Control, and Dynamics*, Vol. 35, No. 1, 2012, pp. 116–128.
- [12] V. G. Szebehely, *Theory of Orbits: The Restricted Problem of Three Bodies*. New York: Academic Press, 1967.
- [13] G. Goméz, *Dynamics and Mission Design Near Libration Points. Volume 3, Advanced Methods for Collinear Points*. Singapore ; River Edge, NJ: World Scientific, 2001.
- [14] K. K. Boudad, D. C. Davis, and K. C. Howell, “Disposal Trajectories From Near Rectilinear Halo Orbits,” *AAS/AIAA Astrodynamics Specialist Conference*, 2018.
- [15] D. C. Davis, C. Patterson, and K. C. Howell, “Solar Gravity Perturbations to Facilitate Long-term Orbits: Application to Cassini,” *AIAA/AAS Astrodynamics Specialist Conference*, 2007.
- [16] K. K. Boudad, K. C. Howell, and D. C. Davis, “Near Rectilinear Halo Orbits in Cislunar Space within the Context of the Bicircular Four-Body Problem,” *AIAA/AAS SciTech Forum*, 2019.
- [17] D. C. Davis, “Multi-Body Trajectory Design Strategies Based on Periapsis Poincare Maps,” *PhD Dissertation*, Purdue University, West Lafayette, Indiana, 2011.
- [18] K. K. Boudad, “Disposal Dynamics from the Vicinity of Near Rectilinear Halo Orbits in the Earth-Moon-Sun System,” 2018. M.S. Thesis, Purdue University, West Lafayette, Indiana.